IEEE Transactions on Quantum Engineering

Received 20 June 2023; revised 2 August 2023; accepted 14 September 2023; date of publication 19 September 2023; date of current version 25 October 2023.

*Digital Object Identifier 10.1109/TQE.2023.3316797*

# Time Binning Method for Nonpulsed Sources Characterization With a Superconducting Photon Number Resolving Detector

**PASQUALE ERCOLANO[1,2], CIRO BRUSCINO[1], DANIELA SALVONI[3], CHENGJUN ZHANG[3], MIKKEL EJRNAES[4], JIA HUANG[5], HAO LI[5], LIXING YOU[5], LOREDANA PARLATO[1,6], AND GIOVANNI PIERO PEPE[1,6]**

[1]Dipartimento di Fisica "E. Pancini," Università degli Studi di Napoli Federico II, I-80125 Napoli, Italy
[2]CNR-INO National Institute of Optics, I-50125 Firenze, Italy
[3]Photon Technology (Zhejiang) Company, Ltd., Jiashan 314100, China
[4]CNR-SPIN Institute of Superconductors, Innovative Materials and Devices, I-80078 Pozzuoli, Italy
[5]National Key Laboratory of Materials for Integrated Circuits, Shanghai Institute of Microsystem and Information Technology, Chinese Academy of Sciences, Shanghai 200050, China
[6]CNR-SPIN Institute of Superconductors, Innovative Materials and Devices, I-80078 Napoli, Italy

Corresponding author: Loredana Parlato (e-mail: loredana.parlato@unina.it).

This work was supported in part by the European Union - PON Ricerca e Innovazione 2014-2020 FESR /FSC - Project ARS01_00734 QUANCOM2.

**ABSTRACT** Photon number resolving detectors find space in many fields, such as quantum optics, boson sampling, and fluorescence spectroscopy. In particular, the reconstruction of the input photon distribution is essential in quantum communications to detect photon-number-splitting attacks. In this work, we discuss the operation configurations of a photon number resolving detector based on superconducting nanostrips at a wavelength of 1550 nm from a temporal point of view. We set a time binning and acquired the number of recorded pulses per bin by means of a time-to-digital converter. We studied the predictions of two theoretical models and compared them to the experimental data in order to analyze their operation regimes depending on the binwidth and to employ them for the reconstruction of the input photon distribution. We applied this method to a continuous-wave laser source, showing that the former can be used for the characterization of nonpulsed light sources, even with a photon emission rate so low that the dark count rate of a superconducting nanostrip is not negligible.

**INDEX TERMS** Light sources, photodetectors, photon number resolving detectors (PNRDs), superconducting devices, superconducting photodetectors.

## I. INTRODUCTION

A detector able to resolve the number of photons is required in numerous applications ranging from quantum communication, such as the detection of a photon-number-splitting attack, to quantum optics, in which n-photon states are commonly employed [1]. By means of a photon number resolving detector (PNRD), indeed, it is possible both to determine the number of incident photons and to reconstruct its distribution [2]. They are already commonly employed in the ultraviolet and visible wavelength regime, but the need to extend the aforementioned applications to the telecom wavelength, at which silicon detectors are blind, has boosted the optimization of PNRD based on superconducting devices. Different superconducting detectors work as PNRD. Among them, we mention the transition-edge sensors (TES) and superconducting nanostrip detectors (SNSPD) [3]. The PNRD based on TES usually consists of an ultralow-temperature superconducting film, such as tungsten (W), which produces a measurable resistive change within a sharp normal to superconducting transition upon photon absorption. With respect to PNRD based on segmented nanostrips, the TES exhibits high detection efficiency and neglectable intrinsic dark counts but also degrades the timing jitter and the maximum count rate. Furthermore, it requires a sub-Kelvin operating temperature. Unlike the TES, SNSPDs, based on the transition of a nanostrip based on relatively high critical

temperature superconductors (NbN, NbTiN, MoSi, WSi, etc..), from the zero voltage state (superconducting state) to the finite voltage (normal state) work at relatively high temperature (a few K in the case of NbN), providing a near unit efficiency at 1550 nm, while having a picosecond time resolution and a few cps dark count rate (DCR) [4], and also other materials are under investigation [5], [6], [7]. By arranging the superconducting nanostrips according to an array, they can independently switch when the photons arrive on the detector. On the basis of the number of switched strips, we can resolve the number of photons. Therefore, the strips act as the pixels of a PNRD [8], [9]. For the reading of their signal, a power combiner can be used, and this has provided good results for the characterization of pulsed sources. In this case, the number of photons is distinguished according to the height of the voltage pulse which is recorded in correspondence with a light pulse arriving from the source [8], [10]. However, the characterization of a continuous, nonpulsed light source can be more intricate. Indeed, since the photons do not hit the detector in temporal separated light pulses, the recovery time of each pixel composing the detector has to be taken into account within the description of the response of the PNRD [11]. An approach proposed by Dauler et al. [11] was based on the record, by an oscilloscope, of the time of registered voltage pulses within a time bin. With a subsequent analysis, the number of pulses recorded by the entire device is reconstructed.

In this work, we take into account a PNRD consisting of an array of eight NbN nanostrips arranged according to a meandered geometry. It is suitable to operate at a temperature of about 2 K and it was realized by Photon Technology (Photec) [12]. While modifying the temporal configuration of the data acquisition, using a time binwidth ranging from a few nanoseconds to several microseconds (and then longer than in [11]), we analyze the performance of these detectors on the basis of two theoretical models by which it is possible both to predict the distribution of the number of recorded pulses and to reconstruct the distribution of the incident photons [13], [14]. The former describes an ideal PNRD, which in principle can detect any number of photons, and whose output is related only to its efficiency and not to an array of segments (single photon detectors), like a TES. Conversely, the latter describes the device taking into account its segmented nature, as composed of single-photon detectors, which in certain conditions arises. In this way, we provide a tool for choosing the best conditions in which the detector works and the most suitable description of it. However, these theoretical models do not take into account the dark counts of the detector, since they assume that they are negligible. For instance, when we use a pulsed light source, during the duration of the pulse the average number of dark counts is typically negligible compared to the one of incoming photons, especially in the case of superconducting nanostrips, which exhibit a very low DCR. However, if we are considering a nonpulsed light source and the emission photon rate is not high enough, the dark counts can negatively affect the predictions of the models. Therefore, we included them in order to take into account continuous light sources with a relatively low photon emission rate, too.

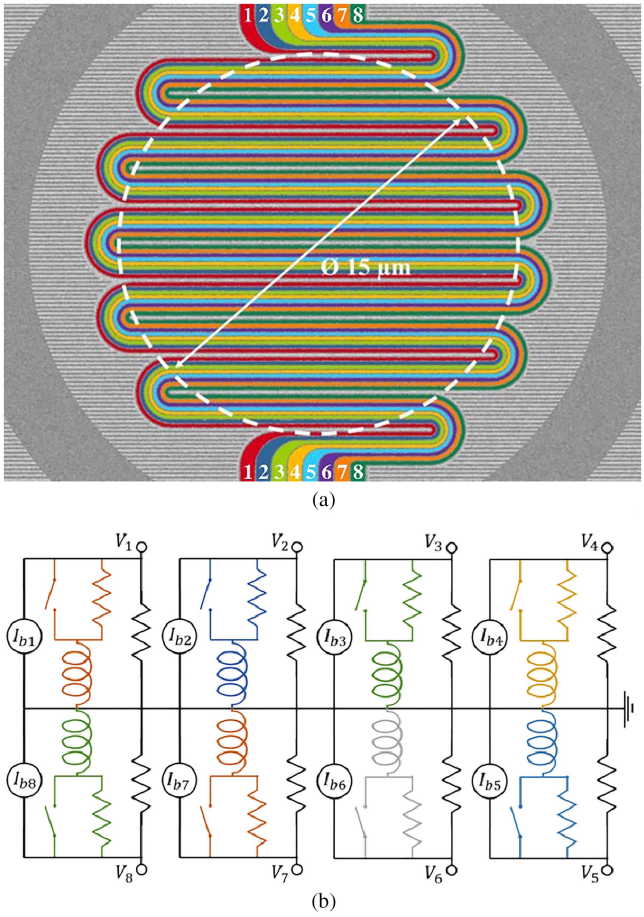


**FIGURE 1. Image of a PNRD with eight pixels. (a) Each nanostrip is represented with a different colour and number. (b) Electrical scheme of a segmented configuration of eight pixels.**

## II. METHODOLOGY

The considered superconducting PNRD is optimized to detect photons whose wavelength is 1550 nm by using an optical cavity [15]. In addition, the meandered geometry of the device [see Fig. 1(a)] ensures that all pixels register about the same count rate when the device is illuminated, and hence they have the same efficiency. Each pixel has a width $w = 75$ nm and a thickness $d = 6$ nm. The active area of the entire device has a diameter equal to 15 $\mu$m.

A schematic picture of the experimental setup is portrayed in Fig. 2. The PNRD is mounted in a closed-cycle Gifford-McMahon cryocooler, whose steady-state temperature is 2.2 K. The temperature is measured by a silicon diode thermometer. The illumination of the device is provided by a single-mode fiber (SMF28e+) mounted on the sample holder containing it. The light source is a continuous-wave laser that emits radiation at 1550 nm with a power of $-20$ dBm. Two variable optical attenuators are arranged after

IEEE Transactions on Quantum Engineering

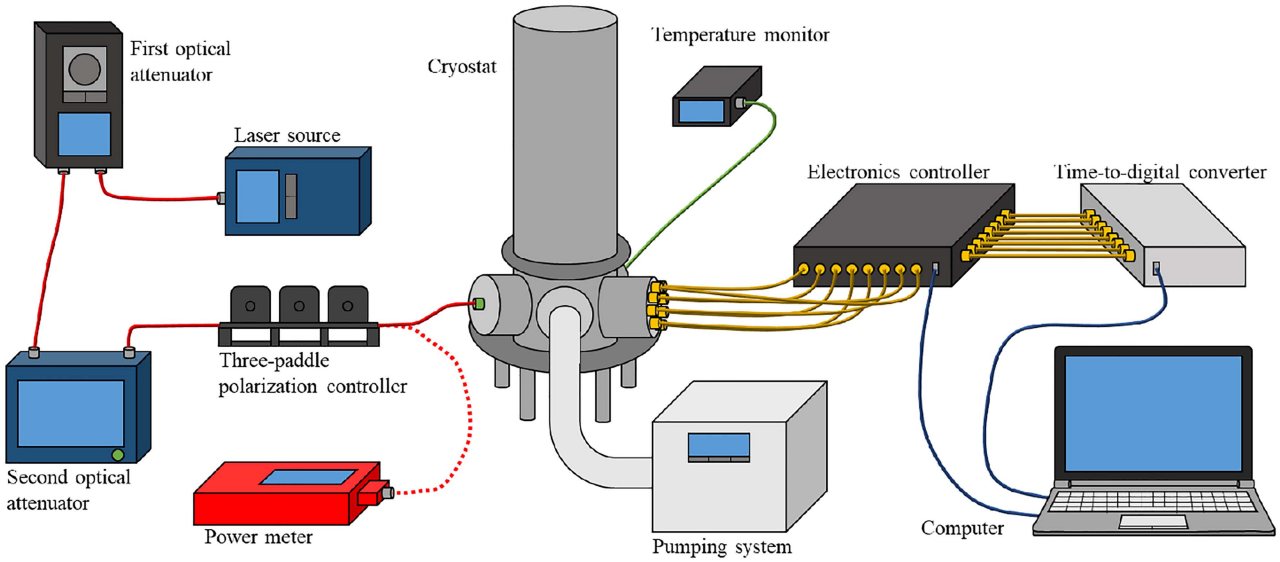


**FIGURE 2.** Scheme of the experimental setup.

the laser source in order to set a lower value of power. A three-paddle polarization controller is employed in order to modify the polarization of the photons and make it parallel to the orientation of the nanostrips. A power meter is used to measure the input power. The electronic connections inside the cryostat are provided by BeCu coaxial cables, whereas outside by stainless steel coaxial cables. The electronics part is managed by a readout and bias controller, which includes bias tees, amplifiers, filters, and photon counters. The output signal goes to a time-to-digital converter (Time Tagger Ultra by Swabian Instruments). Both the electronics controller and the time-to-digital converter are controlled by a computer.

The acquisition is carried out by setting a time binning and counting how many pulses per bin have been recorded by each pixel. Then, we sum them and get the total number of pulses recorded by the entire PNRD in each temporal bin. By repeating this procedure for every bin, we can draw a histogram that reports how many times the detector has recorded a certain number of pulses.

## III. THEORETICAL MODELS

The response description of the PNRD depends on the recovery time $\tau_D$ of its pixels and on the binwidth $\tau_{\text{bin}}$ set for the acquisition. When the latter is much longer than the former, if more than one photon arrives on a pixel of the detector, it can record more than one pulse. Indeed, after the absorption of a photon and the resulting recording of a pulse, the device can recover and be ready to record another one [see Fig. 3(a)]. We assume that in this situation the only characteristic that is necessary to describe the detector is its detection efficiency, so it can be represented as a single not segmented device whose efficiency is $\eta$, understood as the ratio between the number of recorded pulses and the number of the incoming photons. When $n$ photons arrive, the probability $\varepsilon_{mn}$ of recording $m$ pulses is proportional to $\eta^m$, but we have to take into account the contribution of the $n-m$ photons not detected. Since the probability of not detecting a single photon is $1-\eta$, the probability of detecting none is $(1-\eta)^{n-m}$. Finally, since the photons are indistinguishable, we multiply for the binomial factor $\binom{n}{m}$ because it is unknown which $m$ photons among the $n$ have caused the record of the pulses. Therefore, the probability $\varepsilon_{mn}$ is equal to [13]

$$\varepsilon_{mn} = \binom{n}{m} \eta^m (1-\eta)^{n-m} . \tag{1}$$

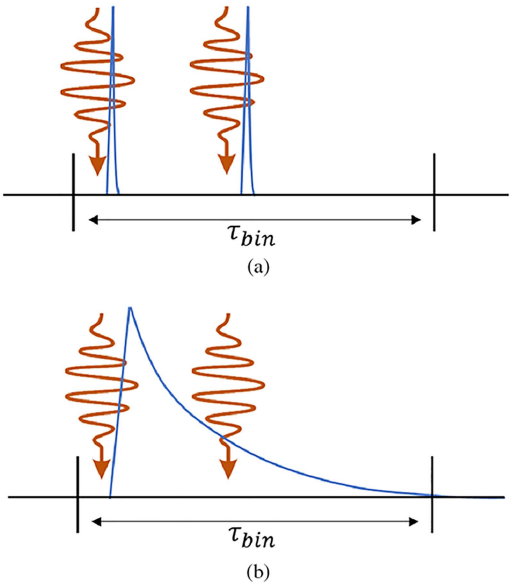


**FIGURE 3.** Summary scheme of the theoretical models. (a) If $\tau_{\text{bin}} \gg \tau_D$, when more than one photon arrives, each pixel can record more than one pulse per bin. (b) If $\tau_{\text{bin}} \approx \tau_D$, each pixel can record at most one count because, after the absorption of a photon and its resulting recording of a pulse, the detector is no longer ready for detection as it has to recover.

As expected, this probability does not depend on the number of segments $N_c$ because we neglected the segmented nature of the PNRD. In addition, since the DCR is not taken into account, the probability of recording a number of pulses higher than the one of the arriving photons is zero. In other words, $\varepsilon_{mn} = 0$ if $m > n$. We included the dark counts in this model according to a recursive approach as in [14]. First, we define the mean number of dark counts per bin of a pixel as $p_{\mathrm{DC}} = \mathrm{DCR} \cdot \tau_{\mathrm{bin}}$, where DCR is referred to a single pixel. Since the segmentation effect is neglectable, the PNRD is described as a single not segmented detector. Therefore, if it consists of $N_c$ segments, its DCR is $N_c \cdot \mathrm{DCR}$. If, we assume that they have a Poissonian distribution, the probability of recording $k$ dark counts in one bin is

$$\rho_{\mathrm{DC}}(k) = \frac{(N_c\ p_{\mathrm{DC}})^k}{k!} e^{-(N_c\ p_{\mathrm{DC}})}. \tag{2}$$

When $n$ photons arrive, the probability of recording $m$ pulses does not only have the contribution $\varepsilon_{mn}$ related to the photon detection, but also the one from dark counts. Indeed, the detector can record $m$ pulses if $k$ dark counts and $m-k$ events due to photons occur, too. Therefore, the probability $\varepsilon'_{mn}$ of recording $m$ pulses when $n$ photons arrive, taking into account also the dark counts, equals to

$$\varepsilon'_{mn} = \sum_{k=0}^{m} \varepsilon_{m-k\ n}\ \rho_{DC}(k)\,. \tag{3}$$

Finally, the probability of recording $m$ pulses is given by [13]

$$P_m = \sum_{n=0}^{\infty} \varepsilon'_{mn} \rho_n \tag{4}$$

where $\rho_n$ is the probability that $n$ photons arrive. Since we neglected the segmented nature of the detector and we described it only through its efficiency, hereafter we will refer to this model as "efficiency only model."

Conversely, when the binwidth is comparable with the recovery time, after a pixel has recorded a pulse, it will no longer be able to record others in the same bin [see Fig. 3(b)]. Therefore, each pixel can record at most one pulse per bin. If the PNRD is made of $N_c$ segments, it can record at most $N_c$ simultaneous pulses. This segmentation effect is not taken into account by the previous model, so some changes are required in order to describe it. In particular, we use the recursive approach presented in [14]. According to the latter, the probability of recording $m$ pulses when $n$ photons arrive can be obtained considering the additional $n$th photon after the previous $n-1$ photons have already arrived. In order to record $m$ pulses, if the detector has already recorded that number of events, the $n$ th photon has to be not detected. Conversely, if the previous $n-1$ photons caused $m-1$ pulses, the last one has to be detected. Therefore, the probability of recording $m$ pulses when $n$ photons arrive is the sum of two contributions [14]

$$\sigma_{mn} = \sigma_{m\ n-1}\left(1 - \frac{N_c - m}{N_c}\kappa\right) + \sigma_{m-1\ n-1}\left(\frac{N_c - (m-1)}{N_c}\kappa\right) \tag{5}$$

where $\kappa$ is the probability, referred to the entire detector, of recording one pulse when one photon arrives. Here, the first addend is the product of the probability of recording $m$ pulses when $n-1$ photons arrive and the one of not detecting the $n$ th photon. Conversely, the second addend is the product of the probability of recording $m-1$ pulses when $n-1$ photons arrive and the one of recording the $m$th pulse because of the $n$ th photon. It is worth to note that, since the segmentation effect is relevant, the number of segments $N_c$ is present. In addition, the probability $\kappa$ is scaled by a factor depending on the number of pixels already switched. Indeed, when a pixel switches, it is no longer able to detect photons, so it does not contribute to $\kappa$ anymore. We assume that each strip contributes in the same way at the probability $\kappa$. Otherwise, the model should then take into account all the different responses of each pixel, as illustrated in [1]. Clearly, the model is much more detailed and heavier from a mathematical point of view, especially for a large number of pixels. The terms of the matrix $\sigma$ can also be written in the compact form [14]

$$\sigma_{mn} = \binom{N_C}{m} \sum_{j=0}^{m} (-1)^j \binom{m}{j} \left((1-\kappa) + \frac{(m-j)\,\kappa}{N_C}\right)^n. \tag{6}$$

It is worth to note that $\eta$ and $\kappa$ are strictly related, but they are not the same quantity. Indeed, the detection efficiency $\eta$ is equal to the ratio between the number of recorded pulses and the number of incoming photons, so it is easily accessible experimentally. $\kappa$ has a higher value because, when more than one photon arrives on the same pixel, the latter can record at most one pulse. Therefore, it misses some counts, and this effect decreases the total number of recorded pulses and hence $\eta$. Thus, $\kappa$ cannot be obtained immediately, but it is related to $\eta$ and to the distribution of the incoming photons $\rho$. In the case of a single strip ($N_C = 1$), it is possible to record at most one pulse, with probability

$$\sigma_{1n} = 1 - (1-\kappa)^n. \tag{7}$$

By definition, the detection efficiency is equal to

$$\eta = \sum_{n=1}^{\infty} \frac{\sigma_{1n}\rho_n}{\mu}. \tag{8}$$

For a laser light source, the photon distribution is Poissonian

$$\rho_n = \frac{\mu^n}{n!} e^{-\mu}. \tag{9}$$

The detection efficiency can be rewritten by substituting (7) and (9) in (8)

$$\eta = \sum_{n=1}^{\infty} \frac{\mu^n e^{-\mu}}{\mu\, n!} - \sum_{n=1}^{\infty} \frac{[\mu\,(1-\kappa)]^n e^{-\mu}}{\mu\, n!}. \tag{10}$$

IEEE Transactions on Quantum Engineering

Hence

$$\kappa = -\frac{1}{\mu}\ln\left(1-\mu\eta\right). \tag{11}$$

This formula can be extended to the case of $N_C$ segments by taking into account that each pixel has a fraction $1/N_C$ of the overall detection efficiency

$$\kappa = -\frac{N_c}{\mu}\ln\left(1-\frac{\mu\eta}{N_c}\right). \tag{12}$$

It is worth to note that, when $\frac{\mu}{N_c} \ll 1$, the first-order Taylor expansion returns $\kappa = \eta$. Indeed, in these conditions, it is very unlikely that more than one photon arrive on the same pixel. Thus, the probability of registering a pulse when a photon arrives is practically equal to the ratio between the number of recorded pulses and the number of incoming photons.

As in the previous model, the DCR is not considered and hence $\sigma_{mn} = 0$ if $m > n$. In this case, in order to include the dark counts, we followed a recursive reasoning as before. However, since the binwidth is comparable with $\tau_D$, we reasoned about the single pixels because the segmentation effect is not neglectable. Since the dark counts are Poissonian events, the probability that a pixel does not record a dark count in a bin is $e^{-p_{\mathrm{DC}}}$, whereas its complementary is $(1-e^{-p_{\mathrm{DC}}})$. Each pixel can only record one pulse or none with these probabilities, respectively. Since the PNRD is made of $N_c$ independent pixels, the probability of recording $k$ pulses when $N$ pixels are ready for detection is binomial

$$\rho_{\mathrm{DC}}(N,k) = \binom{N}{k}\left(1-e^{-p_{\mathrm{DC}}}\right)^k\left(e^{-p_{\mathrm{DC}}}\right)^{N-k}. \tag{13}$$

As before, in order to determine a better estimate of the probability of recording $m$ pulses when $n$ photons arrive, we have to take into account the contribution of the dark counts, too. However, according to the segmentation effect, when $n$ photons cause $m-k$ pixels to switch, only $N_c - m + k$ can record a dark count. Therefore, the expression of this probability becomes

$$\sigma'_{mn} = \sum_{k=0}^{i}\sigma_{m-k\,n}\,\rho_{\mathrm{DC}}(N_c - m + k, k). \tag{14}$$

Then, the probability of recording $m$ pulses becomes [14]

$$P_m = \sum_{n=0}^{\infty}\sigma'_{mn}\,\rho_n \text{ for } 0 \le m \le N_c. \tag{15}$$

It is worthy to note that $m$ ranges from 0 to $N_c$ because, according to this model, each pixel can record at most one pulse per bin. Therefore, the entire PNRD is able to record at most $N_c$ pulses in the same bin. Since this model takes into account the segmented nature of the detector, hereafter we will refer to it as "segmentation model."

At this point, we can also reverse the approach and reconstruct the input photon distribution from the number of recorded pulses. We used the expectation-maximization-entropy (EME) method developed by Hloušek et al. [16]. It is based on an iterative algorithm according to a maximum-entropy principle. The initialization condition is

$$\rho_n^{(0)} = \frac{1}{n_{max}+1} \tag{16}$$

where $n_{\max} \gg \mu$ is the number of terms of the distribution $\rho$ taken into account. At the step $k$, the term $n$ of the input photon distribution is [16]

$$\rho_n^{(k+1)} = \Pi_n^{(k)}\rho_n^{(k)} - \lambda\left(\ln\rho_n^{(k)} - S^{(k)}\right)\rho_n^{(k)}. \tag{17}$$

Here $\lambda$ is a scale factor which we chose equal to $10^{-3}$ as in [16], whereas

$$\Pi_n^{(k)} = \sum_m \frac{P_m\,\theta_{mn}}{\sum_j \theta_{mj}\,\rho_j^{(k)}} \tag{18}$$

$$S^{(k)} = \sum_n \rho_n^{(k)}\ln\rho_n^{(k)}. \tag{19}$$

Here $\theta$ is the matrix that describes the response of the PNRD, namely $\varepsilon'$ or $\sigma'$ depending on the binwidth regime. Conversely, $P_m$ is the probability of recording $m$ pulses, which can be estimated as the ratio between the number of times in which the detector records $m$ pulses and the number of bins.

**TABLE 1. Bias Current at the Setpoint and Related DCR in Addition to the Results of the Fitting Procedure for Each Pixel of the PNRD**

| Pixel | $I_b$ (μA) | $I_c$ (μA) | DCR (Hz) | $\kappa$ (%) | $\tau_D$ (ns) |
|---|---|---|---|---|---|
| 1 | 9.29 | 10.9 | 98 ± 3 | 9.03 ± 0.04 | 5.7 ± 0.1 |
| 2 | 9.20 | 10.8 | 103 ± 2 | 8.88 ± 0.02 | 5.65 ± 0.07 |
| 3 | 9.57 | 10.8 | 101 ± 2 | 9.07 ± 0.02 | 5.60 ± 0.07 |
| 4 | 9.50 | 10.8 | 104 ± 3 | 9.01 ± 0.03 | 5.62 ± 0.09 |
| 5 | 9.41 | 10.8 | 99 ± 2 | 8.77 ± 0.03 | 5.54 ± 0.09 |
| 6 | 9.27 | 10.8 | 103 ± 2 | 8.72 ± 0.03 | 5.55 ± 0.09 |
| 7 | 9.37 | 10.8 | 98 ± 2 | 8.82 ± 0.04 | 5.6 ± 0.1 |
| 8 | 9.41 | 10.8 | 101 ± 2 | 8.96 ± 0.04 | 5.7 ± 0.1 |

## IV. RESULTS

The single pixels were characterized in terms of the current-voltage ($I$-$V$) characteristics. The critical current $I_c$ was determined from the $I$-$V$ curve as the maximum current before the switching to the resistive branch. A measurement of the DCR as a function of the bias current $I_b$ was done and the value of the latter at the operation point was set so that DCR was equal to 100 Hz. The operation bias current and the corresponding DCR are reported in Table 1 for each pixel.

We measured the system detection efficiency (SDE) as the difference between the recorded count rate and the DCR, divided by the input photon rate $\Gamma_{\mathrm{ph}}$. Fig. 4(b) shows the values of SDE as $\Gamma_{\mathrm{ph}}$ increases. It is worthy to note that the SDE of the entire PNRD is higher than 70% up to $\Gamma_{\mathrm{ph}} =$ 10 MHz. Then, it diminishes until it triggers the latching when $\Gamma_{\mathrm{ph}} > 250$ MHz. In Fig. 4(a), the SDE of each pixel is reported. As expected, according to the geometry of the

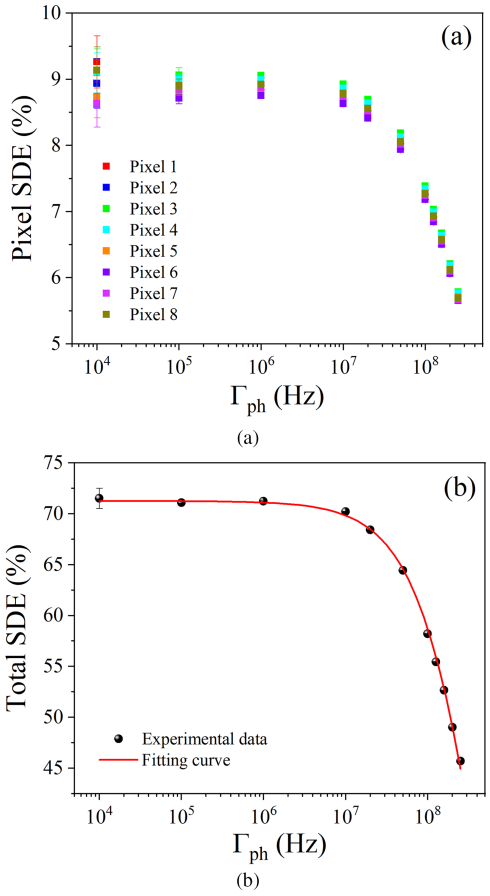


**FIGURE 4.** (a) SDE of the single pixels of the PNRD as the input photon rate $\Gamma_{ph}$ increases. (b) Measured SDE of the entire PNRD (black points) and fitting curve (red line).

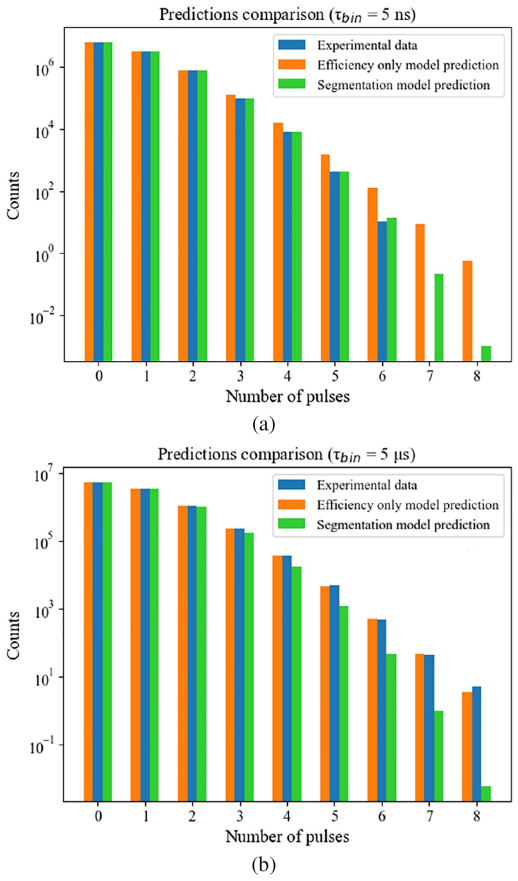


**FIGURE 5.** Histograms reporting the comparison between the recorded counts and the ones predicted by each theoretical model [(3) and (14)], when $\mu = 1$, for different binwidths: (a) $\tau_{\text{bin}} = 5$ ns. (b) $\tau_{\text{bin}} = 5$ $\mu$s. The bins referring to seven and eight pulses in (a) are not filled, in accordance with an average value of the counts less than 1.

PNRD, the efficiency is almost the same for all. This confirms that the device was manufactured uniformly because each strip responds in the same way when it is illuminated by the same light, allowing to use the model proposed in (14). In addition, from (12), we derive

$$\text{SDE} = \frac{N_c}{\tau_C \Gamma_{ph}} \left(1 - e^{-\tau_C \Gamma_{ph} \kappa / N_c}\right) \tag{20}$$

where we rewrote $\mu$ as the product of $\Gamma_{\text{ph}}$ and a characteristic time $\tau_C$. In particular, $1/\tau_C$ provides the characteristic input photon rate $\Gamma_C$ with which the efficiency decreases. By performing a fitting procedure according to (20) on the data referring to the SDE of each pixel, for each of them we got an estimate of $\tau_C$ and the system probability $\kappa$ of recording one pulse when one photon arrives. As we can observe in Table 1, the obtained results are consistent with each other. A fitting procedure of the same type was performed on the SDE of the entire PNRD. The fitting curve is reported in Fig. 4(b). This analysis returned $\tau_C = (45.0 \pm 0.6)$ ns and $\kappa = (71.3 \pm 0.2)$ %. The former corresponds to a characteristic input photon rate $\Gamma_C = (22.2 \pm 0.3)$ MHz. In addition, a recovery time $\tau_D = 6$ ns was estimated by an exponential fit on a voltage pulse recorded by the detector.

The time binning analysis was carried out by modifying the binwidth while keeping the mean number of photons per bin, equal to $\mu = \Gamma_{\text{ph}} \cdot \tau_{\text{bin}}$, constant. In this way, we compared the predictions of the two models with the same Poissonian distribution of the number of photons per bin, but in different temporal configurations.

From a qualitative point of view, we can see from the corresponding histogram [see Fig. 5(a)] that the efficiency-only model is not able to describe correctly the detector when the binwidth is comparable with the recovery time. Indeed, as the number of pulses increases, the agreement is worse and worse because, when more than one photon arrive on the same pixel, the latter will record at most one pulse because it does not have enough time to recover. Therefore, this model overestimates the counts as it does not take into account that our detector has a limited characteristic time which does not allow it to recover from the previous detection event in a bin. Therefore, it predicts that the detector is able to record more than one pulse per bin. Conversely, using the segmentation model, the agreement sensitively improves. When $\tau_{\text{bin}} \gg \tau_D$ [see Fig. 5(b)], the opposite occurs: the segmentation model

IEEE Transactions on Quantum Engineering

is not able to reproduce the experimental data anymore. Indeed, if more than one photon arrives on a pixel, the latter can record more than one pulse. For this reason, the segmentation model underestimates the number of counts, whereas the efficiency-only model well describes the data.

For a quantitative comparison, we evaluated the $\chi^2$ as the sum of the squares of the difference between the experimental counts and the ones predicted by the theoretical model, normalized to the latter

$$\chi^2 = \sum_m \frac{\left(C_m^{\text{experimental}} - C_m^{\text{predicted}}\right)^2}{C_m^{\text{predicted}}}. \tag{21}$$

In Fig. 6, we report the values of $\chi^2$ as the binwidth increases at three different values of $\mu$. When $\tau_{\text{bin}} < 50$ ns, $\chi^2$ is lower for the segmentation model, so the segmentation effect is relevant up to that temporal scale. Conversely, for $\tau_{\text{bin}} > 50$ ns, $\chi^2$ is lower for the efficiency only model. Therefore, the segmentation effect begins to be neglectable and the PNRD begins to be describable as a single detector with efficiency $\eta$. However, if the dark counts are not taken into account as in [14], when $\tau_{\text{bin}}$ increases, the curve relating to the efficiency only model decreases down to a minimum and then increases again. In other words, the agreement with the experimental data is worse and worse. The reason is that when the binwidth increases, in order to have the same $\mu$, we have to reduce the input photon rate. Therefore, DCR is not neglectable anymore and hence the agreement is worse. However, after the introduction of the dark counts, the agreement is sensitively better (see Fig. 6).

According to the model that better suits each binwidth, we can use the EME method in order to reconstruct the input photon distribution and compare it with the expected one, namely the theoretical Poissonian. In particular, for each value of $\tau_{\text{bin}}$, we used in (18) the matrix from the efficiency-only model or the one from the segmentation model depending on which corresponds to a lower value of $\chi^2$. In Fig. 7, the first eight terms of both the theoretical and reconstructed distributions are portrayed.

For a quantitative comparison, we introduce the fidelity

$$F = \left(\sum_n \sqrt{\rho_n^{\text{reconstructed}} \rho_n^{\text{Poissonian}}}\right)^2. \tag{22}$$

By this method, we managed to reconstruct the theoretical distribution with a near unit fidelity (see Fig. 8). As expected from the previous comparison in Fig. 6, the worst configuration to work is 50 ns, at which neither the segmentation model nor the efficiency only model is able to provide an accurate description of the behavior of the detector.

## V. DISCUSSION

The analysis carried out on $\chi^2$ and $F$ brought out three response regimes of the detector. Indeed, since $\chi^2$ has nine degrees of freedom, by setting a significance level of 5%, its upper limit to accept the hypothesis of the model is about

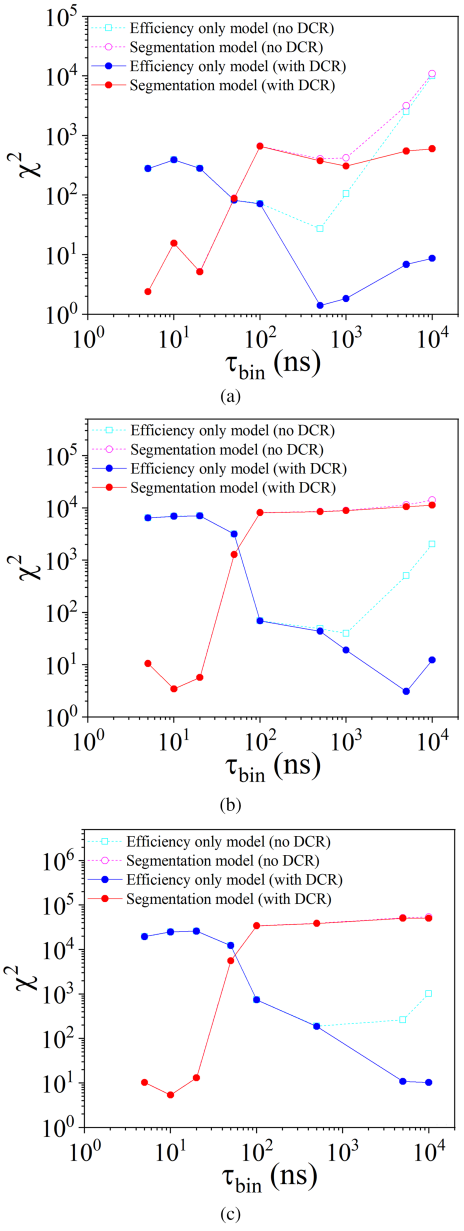


**FIGURE 6. Values of $\chi^2$ for both the efficiency only model and the segmentation model, including [(3) and (14)] or not [(1) and (6)] the dark counts, as the binwidth increases. (a) Is for $\mu = 0.1$, (b) is for $\mu = 0.5$, (c) is for $\mu = 1$.**

17. Therefore, in Fig. 6 we can identify three regions of binwidth values according to the value of $\chi^2$. When $\tau_{bin} < 4\ \tau_D$, $\chi^2$ is acceptable for the segmentation model as each pixel records at most one pulse per bin, except a negligible number of times. In particular, referring to the case of $\mu = 1$, on eighty million time bins considered, when $\tau_{\text{bin}} = 5$ ns, two pulses in a bin on the same pixel have never been recorded, indeed $\tau_{\text{bin}} < \tau_D$. When the binwidth is 10 ns, a pixel detected two pulses in the same bin only twice on eighty million times, whereas an ideal detector, taking into account only its detection efficiency without the effect of the recovery time, should have recorded almost 200 000 events

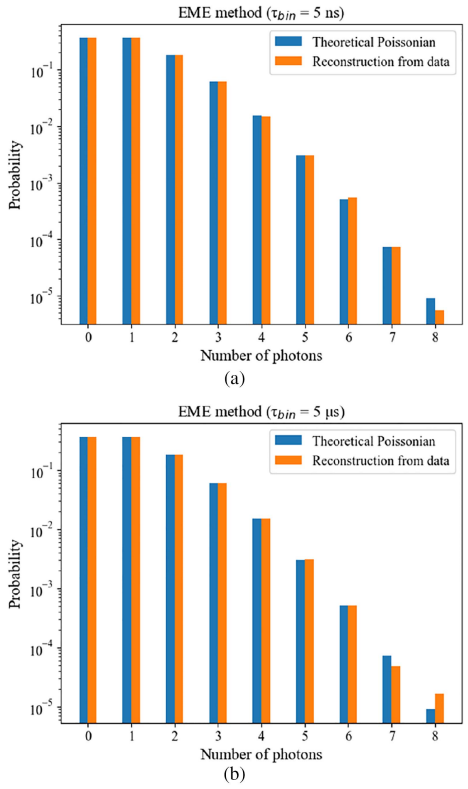


**FIGURE 7.** Histograms reporting the comparison between the first eight terms of the reconstructed input photon distribution and the corresponding terms of the theoretical Poissonian, when $\mu = 1$, for different binwidths. In (a) $\tau_{bin} = 5$ ns, so we used the matrix from the segmentation model. In (b) $\tau_{bin} = 5$ $\mu$s, so we used the matrix from the efficiency only model.

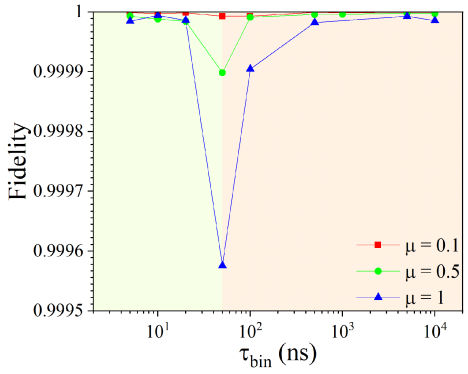


**FIGURE 8.** Values of the fidelity as the binwidth increases. The green area indicates the points for which we used the segmentation model, whereas the red one indicates the points for which we used the efficiency only model.

of this type according to a Poissonian distribution. This event can occur because $\tau_{\text{bin}} = 10$ ns is longer than the recovery time, but it is very unlikely because it requires two photons to arrive at the opposite ends of the time bin, so that the detector records one count at the beginning of the bin and a second one at the ending. Similarly, when $\tau_{\text{bin}} = 20$ ns, this event happened about a thousand times, which is higher than before due to the longer binwidth, but still negligible compared to the 200 000 expected events. This explains why the $\chi^2$ is still acceptable and the segmentation model works at these binwidths. However, for longer binwidths, this probability becomes significant and the model no longer works. For example, when $\tau_{\text{bin}} = 50$ ns, these events occurred about 100 000 times, which is not neglectable anymore as in the previous cases; and even events with three or four photons were observed with this binwidth. However, these values are lower than expected without the recovery time because some photons are not detected as they arrive on the strip when it is not ready. Indeed, the observed 100 000 events are only half of the 200 000 events that an ideal detector would have detected. As the binwidth increases, however, the probability of two photons arriving on the same pixel within the recovery time, for a given mean photon number, decreases until it is neglectable. Therefore, we can ignore the effect of the recovery time and model the detector as always ready for detection, but still with a limited detection efficiency. In other words, in the regime where $\tau_{\text{bin}} \gg \tau_D$, we can characterize the detector by its efficiency only, as an ideal PNRD. This is the reason why the $\chi^2$ is acceptable for the efficiency-only model when $\tau_{\text{bin}}$ is hundred times longer than $\tau_D$. Finally, as described above, in the regime of intermediate binwidths, no model provides a good description of the behavior of the PNRD. $\chi^2$, indeed, is much higher than 17 for both of them. The segmentation model underestimates the number of counts because a pixel may recover and be able to record more than one pulse per bin, and the efficiency-only model overestimates it because some counts are missed if more than one photon hits a pixel within the recovery time.

The same regimes are identified for the fidelity in Fig. 8. When $\tau_{\text{bin}} < 4\ \tau_D$, the segmentationn model provides a fidelity value of approximately 1, as well as the efficiency-only model does when $\tau_{\text{bin}} \gg \tau_D$. Conversely, there is a clear decrease in fidelity for intermediate $\tau_{\text{bin}}$ values. It should be noted that high-fidelity values were obtained in each case. In addition to the model and method employed, the fact that the detection efficiency has been evaluated for each configuration case-by-case contribution, too. Indeed, we measured the input photon rate using the power meter and attenuators: the power meter is calibrated so that $\Gamma_{\text{ph}} = 100$ kHz if the power is $-108.83$ dBm. From this value, we derived the average number of photons per bin multiplying by the binwidth. The efficiency has been measured as the ratio between the total number of pulses recorded (to which we subtracted the ones due to the dark counts, estimated as the product of the DCR, the amplitude of an interval, and the number of intervals) and the product between the average number of photons per interval and the number of intervals. Therefore, we used the same average number of photons both in the theoretical Poissonian and in the calculation of the efficiency, since we measured it. Furthermore, the worsening of the fidelity at intermediate binwidths is less evident for small values of $\mu$, because the multiphoton terms are of little relevance compared to the one photon term. When $\mu$ increases, on the other hand, this decrease is more noticeable because the multiphoton components are relevant.

IEEE Transactions on Quantum Engineering

In conclusion, this analysis has highlighted two regions of work for photon source characterization, namely $\tau_{\text{bin}} < 4\ \tau_D$ e $\tau_{\text{bin}} \gg\ \tau_D$. For sources with a high photon emission rate ($\sim$10 MHz or more), it is better to use short-time bins in order to have a $\mu$ of the order of unity and at most eight simultaneous counts. Indeed, with large bins, we would have a much higher average number of photons per bin, therefore many more terms of the Poissonian to consider. Hence, from a computational point of view, applying the EME method becomes much more cumbersome. Conversely, when the photon emission rate is low ($\sim$100 kHz or less), it is better to use large bins in order to have a sufficiently large average number of photons. Indeed, if we used narrow bins, we would have an average number of photons per bin much smaller than one, and the entire PNRD would almost always record no counts in any bin because the probability of recording multiple counts would be extremely low. Therefore, an extremely large data set would be needed to reconstruct the statistic of the number of incoming photons. This results in a longer acquisition time because the computer has to do many sums of the number of counts recorded by the eight pixels in each bin. Conversely, with long bins, the acquisition of less data is required to fill the histogram bins for more counts, because the average number of photons is higher. However, for continuous light sources with a very low photon emission rate, the dark counts cannot be neglected. For this reason, we also included these ones in the model, and it was shown that the agreement with the data improves significantly. Therefore, the analysis of a nonpulsed laser proposed in this work paves the way for the characterization of other continuous light sources, even with these characteristics.

## VI. CONCLUSION

A superconducting PNRD has been taken into account, demonstrating its potentialities in predicting the number of counts and reconstructing the distribution of the photons emitted by a light source whose wavelength is 1550 nm. We analyzed different operation temporal configurations according to two theoretical models. We managed to determine which model better describes the response of the detector depending on the binwidth, identifying two working regions related to the recovery time of the detector. Finally, by means of the EME method, we reconstructed the input photon distribution with a near-unit fidelity value. This kind of analysis has been performed on a nonpulsed laser source, but it can be extended to the characterization of light sources whose photon distribution is unknown. Indeed, this work has shown that this method is a valid tool for the reconstruction of the statistic of the number of photons emitted by a continuous light source, even with a low photon emission rate by the inclusion of the dark counts in the models which describe the response of the PNRD.

## ACKNOWLEDGMENT

The authors thank professor Weijun Zhang and professor Alberto Orso Maria Iorio for their advice.

*Conflict of Interest:* The authors have no conflicts to disclose.

## REFERENCES

[1] A. Divochiy et al., "Superconducting nanowire photon number resolving detector at telecom wavelength," *Nature Photon.*, vol. 2, no. 5, pp. 302–306, Apr. 2008, doi: 10.1038/nphoton.2008.51.

[2] F. Marsili et al., "Physics and application of photon number resolving detectors based on superconducting parallel nanowires," *New J. Phys.*, vol. 11, no. 4, Apr. 2009, Art. no. 045022, doi: 10.1088/1367-2630/11/4/045022.

[3] A. E. Lita, D. V. Reddy, V. B. Verma, R. P. Mirin, and S. W. Nam, "Development of superconducting single-photon and photon-number resolving detectors for quantum applications," *J. Lightw. Technol.*, vol. 40, no. 23, pp. 7578–7597, Dec. 2022, doi: 10.1109/JLT.2022.3195000.

[4] I. E. Zadeh et al., "Superconducting nanowire single-photon detectors: A perspective on evolution, state-of-the-art, future developments, and applications," *Appl. Phys. Lett.*, vol. 118, no. 19, May 2021, Art. no. 190502, doi: 10.1063/5.0045990.

[5] G. P. Pepe et al., "Novel superconducting proximized heterostructures for ultrafast photodetection," *Cryogenics*, vol. 49, no. 11, pp. 660–664, Nov. 2009, doi: 10.1016/j.cryogenics.2009.02.002.

[6] D. Salvoni et al., "Activation energies in MoSi/Al superconducting nanowire single-photon detectors," *Phys. Rev. Appl.*, vol. 18, no. 1, Jul. 2022, Art. no. 014006, doi: 10.1103/PhysRevApplied.18.014006.

[7] M. Ejrnaes et al., "Single photon detection in NbRe superconducting microstrips," *Appl. Phys. Lett.*, vol. 121, no. 26, Dec. 2022, Art. no. 262601, doi: 10.1063/5.0131336.

[8] W. Zhang et al., "A 16-pixel interleaved superconducting nanowire single-photon detector array with a maximum count rate exceeding 1.5 GHz," *IEEE Trans. Appl. Supercond.*, vol. 29, no. 5, Aug. 2019, Art. no. 2200204, doi: 10.1109/TASC.2019.2895621.

[9] J. Huang et al., "High speed superconducting nanowire single-photon detector with nine interleaved nanowires," *Supercond. Sci. Technol.*, vol. 31, May 2018, Art. no. 074001, doi: 10.1088/1361-6668/aac180.

[10] D. Liu et al., "Photon-number resolving and distribution verification using a multichannel superconducting nanowire single-photon detection system," *J. Opt. Soc. Amer. B*, vol. 31, no. 4, pp. 816–820, Mar. 2014, doi: 10.1364/JOSAB.31.000816.

[11] E. A. Dauler et al., "Photon-number-resolution with sub-30-ps timing using multi-element superconducting nanowire single photon detectors," *J. Modern Opt.*, vol. 56, no. 2–3, pp. 364–373, Feb. 2009, doi: 10.1080/09500340802411989.

[12] PHOTEC, Zhejiang Photon Technology Co., Ltd., 2023. [Online]. Available: https://www.cnphotec.com/

[13] M. O. Scully and M. S. Zubairy, "Photon counting and photon statistics," in *Quantum Optics*. Cambridge, U.K.: Cambridge Univ. Press, 1997, ch. 4, sec. 4.5, pp. 137–138.

[14] M. J. Fitch, B. C. Jacobs, T. B. Pittman, and J. D. Franson, "Photon-number resolution using time-multiplexed single-photon detectors," *Phys. Rev. A*, vol. 68, no. 4, Oct. 2003, Art. no. 043814, doi: 10.1103/PhysRevA.68.043814.

[15] H. Li et al., "Improving detection efficiency of superconducting nanowire single-photon detector using multilayer antireflection coating," *AIP Adv.*, vol. 8, no. 11, Nov. 2018, Art. no. 115022, doi: 10.1063/1.5034374.

[16] J. Hloušek, M. Dudka, I. Straka, and M. Ježek, "Accurate detection of arbitrary photon statistics," *Phys. Rev. Lett.*, vol. 123, no. 15, Oct. 2019, Art. no. 153604, doi: 10.1103/PhysRevLett.123.153604.